Clays Clay Miner.,Vol. 70, No. 1:135–153, 2022
https://doi.org/10.1007/s42860-021-00171-4

ORIGINAL PAPER

Petro-Mineralogical and Geochemical Evaluation of Glauconitic Rocks of the Ukra Member (Bhuj Formation), Kutch Basin, India

Saurabh Shekhar · V. Kumari · S. Sinha · D. Mishra · A. Agrawal · K. K. Sahu

Accepted: 15 December 2021

Abstract Glauconites occurring within the Ukra Member of Kutch Basin have remained unexplored in terms of their economic significance. The present study aimed to present a detailed physicochemical characterization of glauconite occurring in the siliciclastic rocks of Guneri and Umarsar area of the Kutch district, Gujarat, India to explore their economic potential. The study involved an integrated petrographical, mineralogical, and geochemical investigation of glauconitic rocks to highlight the occurrence, nature, and maturity of glauconite. The characterization was carried out using X-ray diffraction (XRD), X-ray fluorescence (XRF), and electron probe microanalysis (EPMA) combined with energy dispersive X-ray (EDX), Field emission gun scanning electron microscopy (FEG-SEM), Fourier-transform infrared spectroscopy (FTIR), and inductively coupled plasma mass spectroscopy (ICP-MS). Petrographic and bulk XRD analysis revealed that the glauconite occurs as green pellets constituting ~30 and 40% of the glauconitic sandstone and shale, respectively. Whole-rock analysis showed that the value of K_2O varies considerably from 3.93 wt.% (sandstone) to 5.63 wt.% (shale). Mineral chemistry indicated the distinctive chemical composition of glauconite pellets containing 7.4–8.4 wt.% of K_2O. The parameters, such as the distance between the (001) and (020) peaks and the large K_2O content (~8 wt.%) of the glauconite fraction reflect an evolved to highly evolved stage of maturation. The morphological and spectral signatures further support the high degree of maturation in glauconites. Trace-element analysis implied that the glauconitic sandstone and shale contain elements such as Zn, Mn, Cu, Co, Mo, and Ni, which serve as essential micronutrients for plants. These data sets collectively constitute part of a preliminary study which is prerequisite to beneficiation, but further evaluation of its potential as a potash fertilizer also is needed.

Keywords Geochemistry · Glauconite · Mineralogy · Petrography · Potash Fertilizer

S. Shekhar · S. Sinha · D. Mishra · A. Agrawal · K. K. Sahu
CSIR-National Metallurgical Laboratory, Jamshedpur 831007, India

S. Shekhar · K. K. Sahu (✉)
Academy of Scientific and Innovative Research (AcSIR), Ghaziabad 201002, India
e-mail: drkksahu@yahoo.com

V. Kumari

Indian Institute of Science Education and Research Bhopal, Bhopal 462066, India

Introduction

Glauconite is a dioctahedral, 2:1 interlayer-deficient green mica with a representative chemical formula of $K_{0.8}\ R^{3+}_{1.33}R^{2+}_{0.67}Al_{0.13}Si_{3.87}O_{10}(OH)_2$ (Rieder et al., 1998). The term 'glauconite' is defined by the IMA

(International Mineralogical Association; Rieder et al., 1998) and by the AIPEA (Association Internationale Pour l'Étude des Argiles; Bailey, 1980) as an Fe-rich, interlayer-deficient mica with low Al tetrahedral substitution and K^+ as the dominant interlayer cation (>0.6 atoms per formula unit, apfu). The mineral glauconite exhibits a basal reflection (001) between 14 and 10 Å, (020) reflection at 4.53 Å, (003) reflection at 3.33 Å, and (060) reflection at 1.51 Å (AIPEA; Bailey, 1980). Structurally, glauconite consists of a 2:1 layer (two tetrahedral sheets facing one octahedral sheet) connected with interlayer K^+ cations. Si(IV) cations occupy the tetrahedral sites with the occasional substitution of Al(III) and Fe(III), whereas Fe(III) occupies the octahedral sites, along with Al(III) and significant amounts of divalent cations (Mg(II) and Fe(II)) (Bentor & Kastner, 1965; Hassan & Baioumy, 2006; Srasra & Trabelsi-Ayedi, 2000).

Glauconite is considered as a common authigenic mineral which forms generally during marine transgressive events (Amorosi, 1995; Banerjee et al., 2016a; Bansal et al., 2017, 2018). Occurrences of glauconite in lacustrine and alluvial deposits have also been found, however (McRae, 1972). The origin and evolution of glauconites have been explained by multiple theories such as "layer lattice" theory, "pseudomorphic replacement" theory, and "verdissement" theory (Banerjee et al., 2019; Burst, 1958; Dasgupta et al., 1990; Hower, 1961; Odin & Matter, 1981). The evolution and maturation of glauconite is a diagenetic phenomenon that depends on the K_2O wt.%, as K content evolves with maturation. At the nascent stage, glauconite contains ~2–4 wt.% K_2O, and, subsequently, the K_2O content reaches >8 wt.% for highly evolved glauconites (Amorosi, 1995; Odin & Matter, 1981). Glauconitic rocks release potassium during pedogenesis and weathering processes which help in maintaining soil fertility. Glauconitic rocks with large K_2O contents, therefore, are considered potential sources of potash fertilizers. High soil-water holding capacity and cation exchange capacity compared to other K-bearing silicate rocks such as nepheline syenites (El-Habaak et al., 2016; Manghnani & Hower, 1964a, 1964b; Rahimzadeh et al., 2015) make it an alternative resource of potassium. Other than the direct application of glauconitic rocks as a fertilizer, several methods have been suggested for effective recovery of potassium as a highly soluble salt from glauconitic rocks (Karimi et al., 2012; Rudmin et al., 2017, 2019; Shekhar et al., 2017a, b; Shekhar et al., 2020).

India's limited availability of potassium-rich sea brine and evaporite-hosted potash deposits makes it dependent on foreign countries to meet its potassium fertilizer demand. Due to the lack of conventional potash resources and increasing demand, glauconitic rocks are now being exploited as an alternative indigenous source of potassium in India (Kumar & Bakliwal, 2005; Soni, 1990). The wide occurrence of glauconite deposits is reported from Precambrian rocks of Karnataka, Andhra Pradesh (A.P.), Uttar Pradesh (U.P.), Madhya Pradesh (M.P.), Rajasthan, and Uttarakhand. The Cretaceous rocks of Gujarat, especially those of the Bhuj Formation, contain significant amounts of of glauconite. In addition, the Cretaceous, Eocene (Ladakh, Guajarat, Garhwal, Rajasthan, and Assam), and Recent rocks (Trivandrum coasts, Bay of Bengal, and the coasts of Andaman Nicobar Island) also contain glauconites. Many studies have been carried out to understand the mineralogy, morphology, occurrence, nature, and other physicochemical properties of glauconitic rocks (Amorosi, 2013; Baldermann et al., 2012; Banerjee et al., 2019; Dooley, 2006; Drits et al., 2010; Essa et al., 2016; Franzosi et al., 2014; Harder, 1980; Hower, 1961; Huggett & Gale, 1997; Kelly & Webb, 1999; McRae, 1972; Odin & Matter, 1981; Schimicoscki et al., 2020; Stille & Clauer, 1994; Tang et al., 2017a, b; Thompson & Hower, 1975; Van Houten & Purucker, 1984; Wigley & Compton, 2007). Few published studies exist about glauconitic rocks from India in this context (Banerjee et al., 2008, 2012a, b; Bansal et al., 2020; Choudhuri et al., 1973; Rawlley, 1994; Soni, 1990). The glauconitic rocks of Rajasthan, M.P., U.P., and A.P. have been studied in detail in terms of characterization (Banerjee et al., 2015, 2016a, b; Bansal et al., 2020; Janardhana Rao et al., 1975; Mandal et al., 2020; Mishra et al., 1987); the glauconite deposits of Gujarat have so far only been studied for other aspects such as their composition, origin, and age (Banerjee et al., 2012a, b; Bansal et al., 2017, 2018; Chattoraj et al., 2009; Kuran & Sahiwala, 1999).

The glauconitic belts occurring in the Ukra Member (Bhuj Formation) are abundant in the Kutch area. The glauconites from the type locality have been studied for information on the composition and origin, with limited characterization work to explore the

https://doi.org/10.1007/s42860-021-00171-4 Published online by Cambridge University Press

economic potential of the glauconites. In addition, the glauconitic horizons of the Ukra Member exposed in other areas such as the Guneri and Umarsar remain uninvestigated for their physicochemical characteristics. The aim of the present study, therefore, was to characterize the glauconitic rocks exposed near the Guneri and the Umarsar area of the Kutch district, Gujarat, India, and to explore their geological, mineralogical, and geochemical attributes to gain a better insight into the occurrence, nature, and stage of maturation of the glauconites, which is an essential step in determining their potential to serve as a source of potash fertilizer.

Geological Background

The Kutch basin is a pericratonic rift basin that evolved in the western margin of the Indian subcontinent during the end of the Triassic period. The onset of the breakup of Gondwanaland in the Late Triassic–Early Jurassic period caused reactivation of pre-existing discontinuities along the Aravalli-Delhi trend and opening of the Kutch basin (Biswas, 1987). The basin is asymmetric in geometry with a southward slope and several uplands as well as low land features (Biswas, 1987). The riftogenic basin has hosted predominantly Mesozoic sedimentary sequences (~3000 m) and Post-rift Cenozoic sediments. The Mesozoic rift-fill sediments constituting a major part of the basin were deposited in both marine and non-marine settings (Biswas, 2005). Apart from these sedimentary fills, the basin exposes Deccan traps formed by the emplacement of magma through the faults generated under the extensional settings (Paul et al., 2008). The lithostratigraphic succession of the Kutch basin comprises the Jhurio, Jumara, Jhuran, and the Bhuj formations (Biswas, 1977). The Mesozoic sequence started with the non-marine siliciclastic facies followed by marine siliciclastics, carbonates, and mixed carbonate-siliciclastic sediments (Fürsich & Pandey, 2003). Bhuj Formation is the stratigraphically youngest unit composed dominantly of feldspathic and ferruginous sandstone deposited in marine to non-marine environments (Desai, 2013; Desai & Saklani, 2012). The Bhuj sediments are deposited in a deltaic environment with a pulse of marine transgression. The Bhuj Formation is further subdivided into three members: Guneri, Ukra, and Upper Member.

The siliciclastic rocks of the present study belonging to the Ukra Member of the Bhuj Formation are exposed near the Guneri (23°46’55.3"N, 68°52’17.4"E) and the Umarsar (23°46’5.6"N, 68°50’17.7"E) areas (Fig. 1). However, the type section of the Ukra Member is a 34 m-thick exposure at the base of the Ukra hill (Desai, 2013). The Ukra Member consists primarily of calcareous glauconitic shales and sandstones, which are rich in ammonites, belemnites, gastropods, and wood-log remains (Bansal et al., 2017). Based on the facies association and paleontological evidence, this member is considered as a transgressive tongue in a prograding deltaic sequence (Desai, 2013).

In the Guneri area, the vertical section (~85 cm) exposed in a pit (Fig. 2a) has a well developed glauconite-bearing, fine-grained sandstone which is overlain by hard bands of feldspathic and ferruginous sandstone (Fig. 2e). In contrast, a ~1.2 m-thick sequence near the Umarsar area is characterized by alternating bands of ferruginous sandstone and glauconitic shale (Fig. 2b and f). Generally, the bedded sandstone is the host rock for the glauconites of the Guneri area and the ~1.5 m-thick glauconite band is traceable for up to 3–4 km along the strike (Jain, 1997).

Materials and Methods

Materials

The glauconite-bearing rock samples collected from the Guneri and Umarsar areas of the Kutch district, Gujarat, were investigated in the present work. The glauconitic rock samples studied were collected from pits and a trench at depths of 0.8 and 1.2 m, respectively (Fig. 2a, b). The glauconite sample collected from Guneri occurs in sandstone whereas the sample from Umarsar occurs in shale. Chemicals such as sodium carbonate, sodium bicarbonate, sodium dithionite, sodium citrate dihydrate, acetic acid, hydrofluoric acid, nitric acid, and hydrogen peroxide used for the characterization were of analytical grade and were obtained from Merck (Darmstadt, Germany).

https://doi.org/10.1007/s42860-021-00171-4 Published online by Cambridge University Press

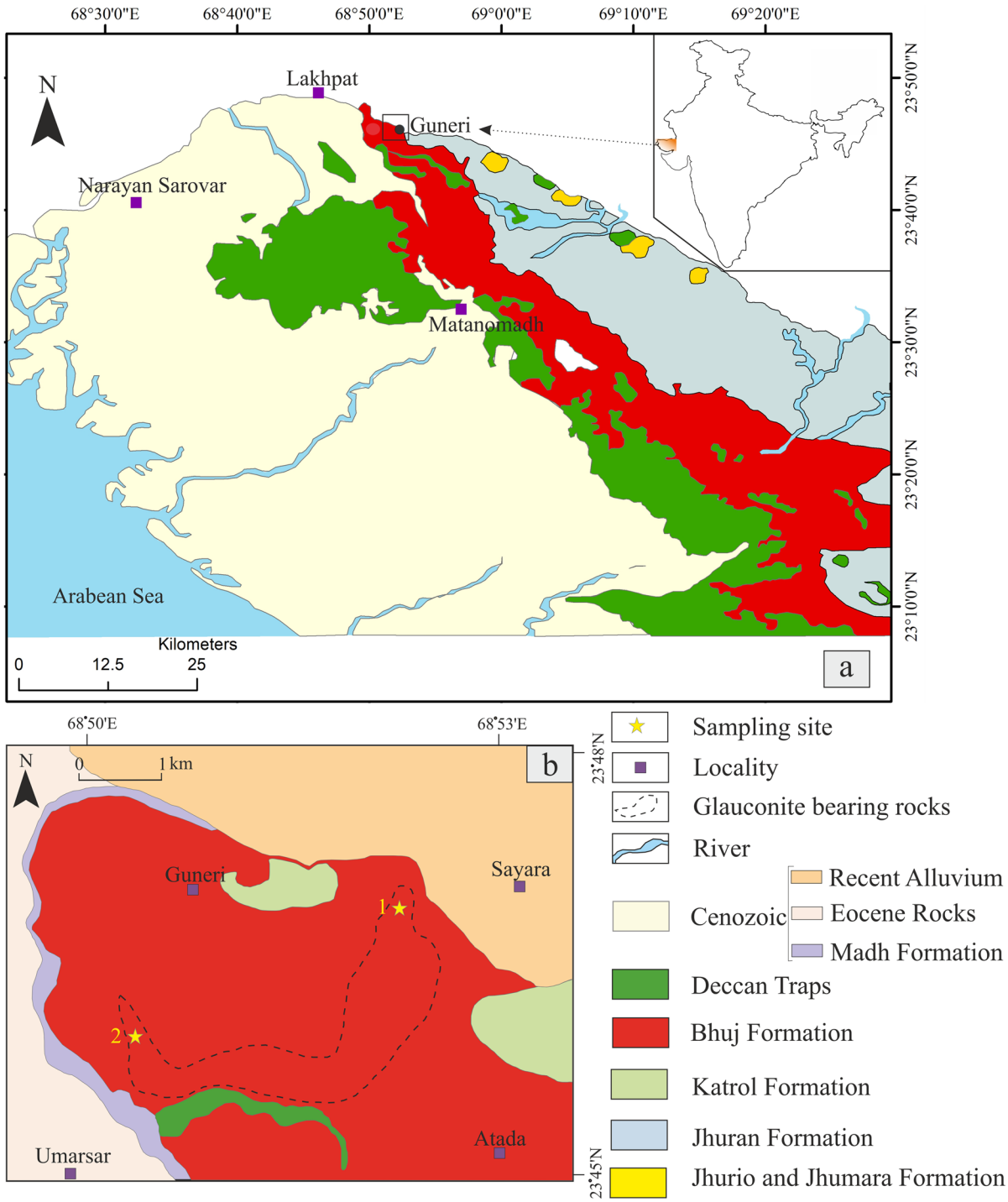

Fig. 1 **a** Geological map of Kutch basin showing the location of the study area; inset map of India shows the study area (map adapted from Bansal et al., 2017). **b** Detailed geological map of the study area showing the sampling locations, which fall in a part of Toposheet No. 41 A/13. The dashed line marks the extent of glauconite-bearing rocks associated with the Bhuj Formation (adapted from Jain, 1997)

https://doi.org/10.1007/s42860-021-00171-4 Published online by Cambridge University Press

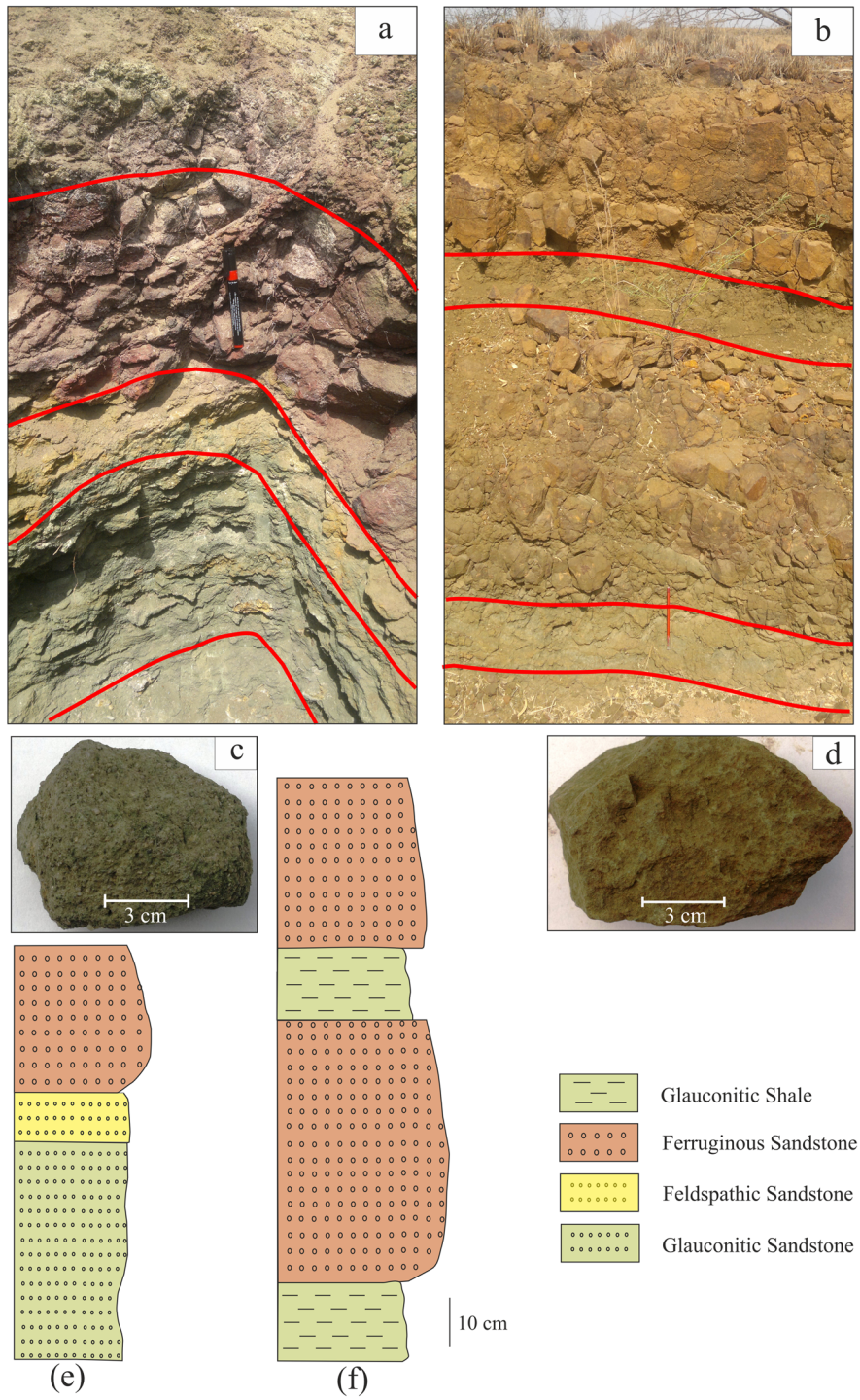

Fig. 2 **a** ~85 cm-thick section exposed near Guneri (sampling site 1 of Fig. 1b) (Shekhar et al., 2017b). The litholog **e** corresponds to this particular section. **b** The exposure at sampling site 2 (Fig. 1b) has a thickness of ~1.2 m. The lithocolumn for this section is shown in Fig. 2f. **c** Glauconitic sandstone sample collected from the site near Guneri. **d** Glauconitic shale sampled from the Umarsar area

https://doi.org/10.1007/s42860-021-00171-4 Published online by Cambridge University Press

Methods

Thin-section preparation for petrographic and electron probe microanalysis The collected rock samples were cut into small chips. The fragile rock chips were hardened by epoxy solution in a vacuum impregnation unit. The samples were kept in a vacuum chamber for 10 min under 80–100 kPa and cured for 12 h (Innes & Pluth, 1970). The hardened rock chips were cut, ground, and smoothed with 220, 600, 800, and 1000 grit carborundum. The chips were mounted on borosilicate glass slides, 4.7 cm×2.5 cm in size, using epoxy as the adhesive. The mounted samples were processed using a PetroThin instrument (semi-automatic thin-sectioning device) to cut the thin section and then ground with 1000 grit carborundum to attain the correct thickness (30 μm). Grinding of the thin section was followed by polishing using 6, 3, and then 1 μm diamond pastes (Innes & Pluth, 1970). The final polished thin section was then ready for petrographic and electron probe microanalysis.

Clay fraction (<2 μm) separation The rock samples were crushed, ground, and sieved using a 300 μm (50 mesh ASTM) sieve. A representative sample was selected from the bulk by coning and quartering. The separation of clay fractions from the bulk sample required pre-treatments for the removal of iron oxide, carbonate, and organic matter, followed by the fractionation procedure. To yield ~5 g of clay fraction, a 20 g portion of each sample was transferred to 250 mL beakers. Iron oxide was removed from the samples using the citrate bicarbonate dithionite (CBD) method (Jackson, 1979). The residues were further treated with 10% acetic acid to remove carbonates, and the organic particles were removed by treating the residue with 30% H_2O_2. Each treatment step included washing the residues using double distilled water. The final residue obtained after treatment was transferred to a 1000 mL graduated cylinder filled with distilled water, dispersed well, and then allowed to sediment following Stokes law. The clay fractions (<2 μm) were separated after the appropriate time interval (~6 h) by removing the suspension, following the method of Soukup et al. (2008). The removed suspension was used to prepare oriented mounts for analysis by XRD and for other characterization studies.

Characterization techniques The hand specimens collected were subjected to mild grinding using a mortar and pestle followed by treatment with anhydrous sodium carbonate. The samples were washed and oven dried for 12 h. Grains were broken and a stereo zoom microscope (Leica-wild M8, Wetzlar, Germany) was used to identify the glauconite and other associated minerals. Microscopic analysis of petrographic thin sections was carried out using a Leica DM 4500P polarizing microscope (Chiyoda-ku, Japan) connected to a Leica DFC420 camera under both transmitted and reflected light. The polished thin section after carbon coating was analyzed using a JEOL-JXA-8230 EPMA (JEOL, Toyko, Japan) with an attached EDX detector; the accelerating voltage was 15 kV, beam current was 4 nA, and the working distance was fixed at 11 mm. The XRD patterns for the bulk-rock samples and the clay fractions were obtained using a Bruker D8 Discover X-ray diffractometer (Bruker GmbH, Bremen, Germany), using Ni-filtered CuKα radiation at a voltage of 40 kV and a current of 40 mA. Bulk samples and clay fractions were scanned over the ranges 5–80 and 0–45°2θ, respectively, with a step size of 0.02°2θ at a scanning speed of 1 s/step. The XRD analysis of oriented samples (clay fractions) was perfomed on samples which were air-dried (AD), exposed to ethylene glycol (EG) vapor, and heated at 550°C. All samples were analyzed under the same operating conditions. The PANalytical *X'Pert HighScore Plus* Software and the JCPDS database were used for mineral identification. Clay fractions were scanned using an FEI Nova NanoSEM 430 (Waltham, Massachusetts, USA) scanning electron microscope (SEM) to study the morphology. The SEM was operated in high-vacuum mode (10^{-3} Pa) with 15 kV operating voltage. Infrared vibrational spectra were recorded using an Alpha-Bruker FTIR spectrometer (Billerica, Massachusetts, USA) in the middle infrared (MIR) range (4000–500 cm^{-1}).

Major oxides of bulk samples were determined using X-ray fluorescence spectrometry (Bruker SRS 3400, Bremen, Germany) with analytical uncertainties of <5%. Trace-element concentrations of glauconitic sandstone and shale were measured using an inductively coupled plasma mass spectrometer (ICP-MS, Agillent, Santa Clara, California, USA). For ICPMS analysis, ~25 mg of each powdered whole-rock sample was digested using a mixture of HF+ HNO_3 for 48 h at 120°C. The digested samples

https://doi.org/10.1007/s42860-021-00171-4 Published online by Cambridge University Press

were diluted to 100 mL in 2% HNO_3 solution which was spiked with 10 ppb In, Cs, Re, and Bi (internal standards). The USGS standard reference materials (SRMs) BCR-2, BHVO-2, GSP-2, and AGV-2 were used for calibration. BCR-2 (basalt) and GSP-2 (granite) USGS rock standards were run as unknowns for the estimation of accuracy. The analytical uncertainties (2σ error) were <5% for trace elements.

Results and Interpretation

Petrographic Study of Glauconitic Rocks

Petrographic observation indicated that glauconite occurs in medium- to fine-grained sandstone as well as in shale. Glauconite occurs as pellets that are mainly globular, irregular, oval, ellipsoidal, or lobate in shape. The thinly laminated glauconitic sandstone is composed primarily of sub-angular to sub-rounded quartz and glauconite (Fig. 3a). Glauconitic sandstone contains mostly monocrystalline quartz which floats in the matrix and constitutes 60 to 65% of the sample by volume (Fig. 3a).

Glauconite constituting ~25–30% of the sample can be considered as the second major component after quartz in glauconitic sandstone. Well rounded glauconite pellets have diameters ranging from 0.25 to 0.5 mm (Fig. 4a, b). The light to dark green-colored glauconite present in sandstone exhibits pleochroism from yellowish green to dark green (Fig. 3a). It shows high-order yellowish green to dark green interference colors under crossed polars (Fig. 4b). Glauconitization was observed along the cleavage planes and fractures of feldspar grains. Glauconitic pellets filling the voids indicated their formation by replacement of K-feldspar (Baldermann et al., 2017; Bansal et al., 2017). A few grains of glauconite had toothed or lacerated margins, which ruled out long-distance transport of these grains in the sandstone (Fig. 4a, b). The presence of fractured and broken pellets in the sandstone indicated the highly evolved nature of the glauconite (Amorosi, 2012; Baldermann et al., 2012, 2017; Bansal et al., 2017; Chamley, 1989; Odin & Matter, 1981). The relative abundance of dark green glauconite grains in the sandstone also indicated the evolved nature of glauconite (Baldermann et al., 2012, 2013, 2017). The highly fractured and highly evolved nature of the glauconite suggests an autochthonous origin of the glauconite in the sandstone (Baldermann et al., 2017; Li et al., 2012).

In contrast, glauconitic shale was composed of 25–35% of moderately sorted, sub-rounded fine grains of quartz, 20–25% of iron oxide, and 35–40% of sub-angular to sub-rounded, ellipsoidal to elongated glauconite pellets by volume (Fig. 3b). Glauconitic shale had a predominance of yellowish green (light green) glauconite pellets 0.15–0.52 mm in size (Fig. 4c, d). Glauconite in shale shows faint pleochroism under PPL and third-order interference colors under XPL (Fig. 4d). Compositionally, the two varieties are

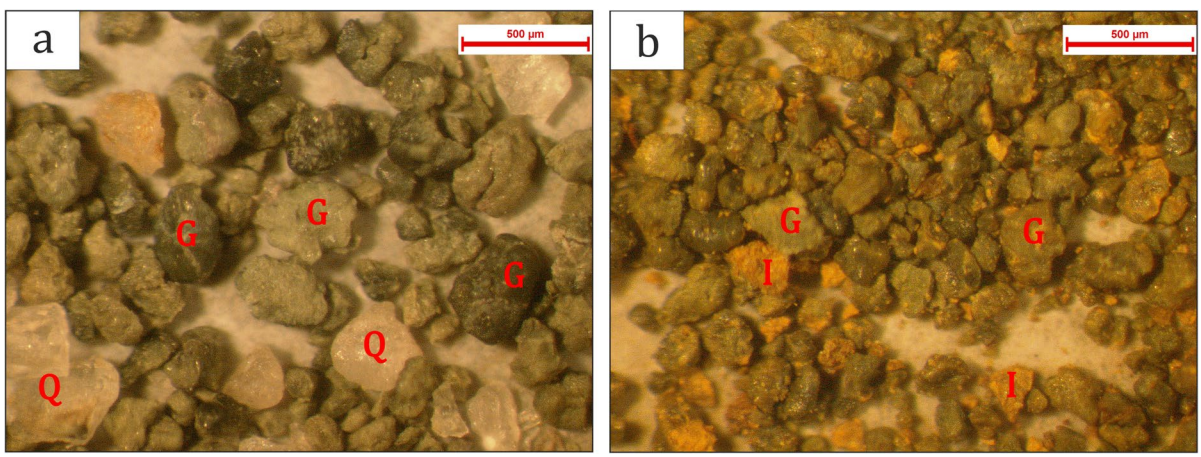

Fig. 3 Stereo zoom microscope image of **a** glauconitic sandstone and **b** glauconitic shale. G: Glauconite, Q: Quartz, I: Iron oxide

https://doi.org/10.1007/s42860-021-00171-4 Published online by Cambridge University Press

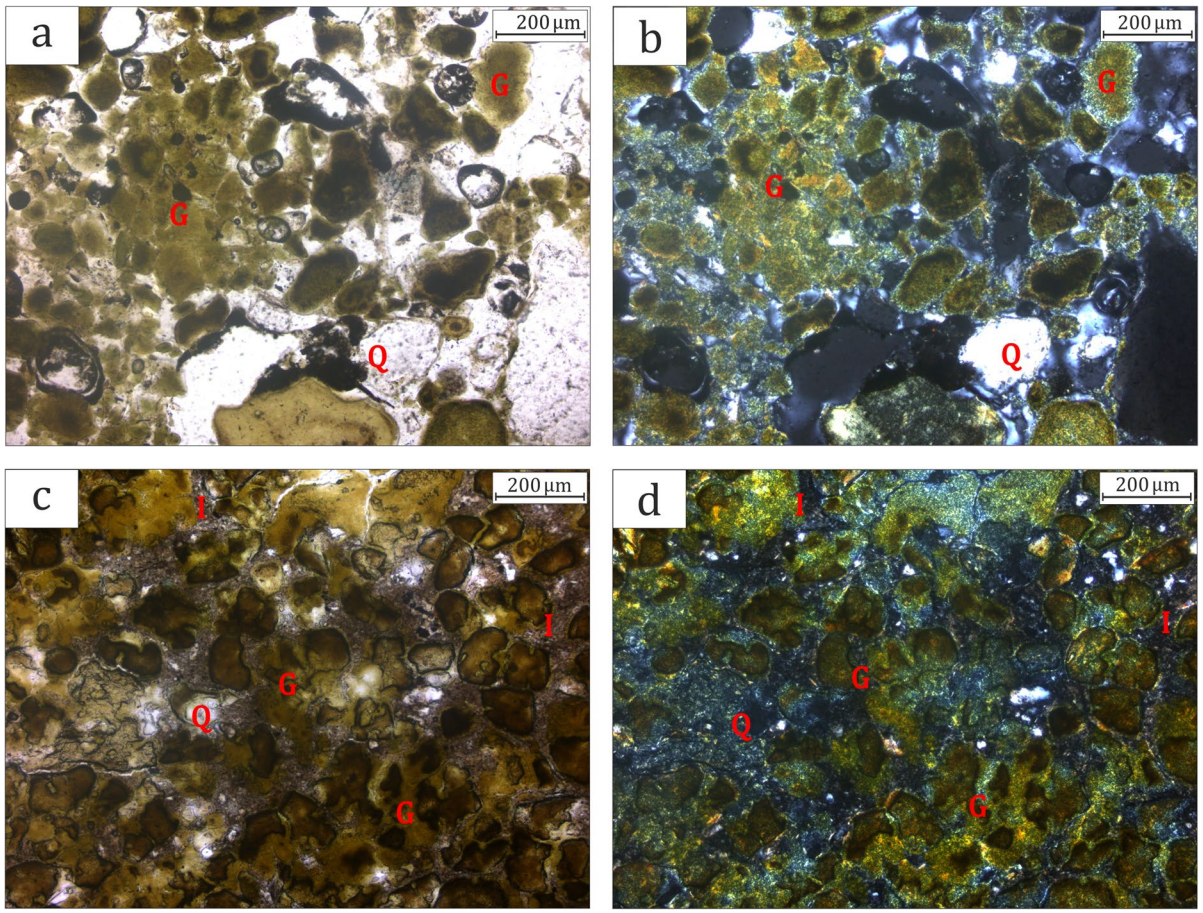

Fig. 4 Photomicrograph of glauconitic sandstone in **a** plane polarized light (PPL) and **b** cross polarized light (XPL) showing glauconite pellets (G) and floating quartz grains (Q). Photomicrograph of glauconitic shale in **c** (PPL) and **d** (XPL) showing glauconite pellets (G), quartz grains (Q), and ferruginous matrix (I)

similar except for the proportion and size of glauconite pellets, which vary significantly in thinly laminated glauconitic sandstone and fine-grained glauconitic shale. Glauconite pellets are quite elongate and ellipsoidal in shape and embedded as randomly oriented pellets within quartz in glauconitic shale. Fractured glauconite pellets are very similar to the glauconite present in the sandstone layer, which also indicated formation by replacement of K-feldspar. The relatively large amount of glauconite in shale further supports this interpretation. The highly fractured and evolved nature suggests that these glauconites must have formed in situ (Amorosi, 1995; Baldermann et al., 2017; Li et al., 2012).

Whole-Rock Mineralogical and Chemical Compositions

The XRD patterns show that quartz (3.34, 4.26, 2.28, 2.13, 1.98, 1.82, 1.54, 1.38, 1.37 Å), glauconite (10.1, 4.53, 3.63, 3.09, 2.58, 2.41, 1.51 Å), feldspar (3.18, 4.13 Å), and iron oxide (3.66, 2.69, 1.69 Å) constitute the bulk mineralogy of the glauconitic rocks (Fig. 5). Semiquantitative estimation based on the method proposed by Kübler (1983) revealed that the sandstone has an abundance of quartz (~65%) followed by glauconite (~30%) and feldspar (5%), whereas the shale sample contained ~40% glauconite. XRD peaks indicated that shale contains relatively less quartz (30%) and showed peaks of iron oxide (hematite ~25%).

https://doi.org/10.1007/s42860-021-00171-4 Published online by Cambridge University Press

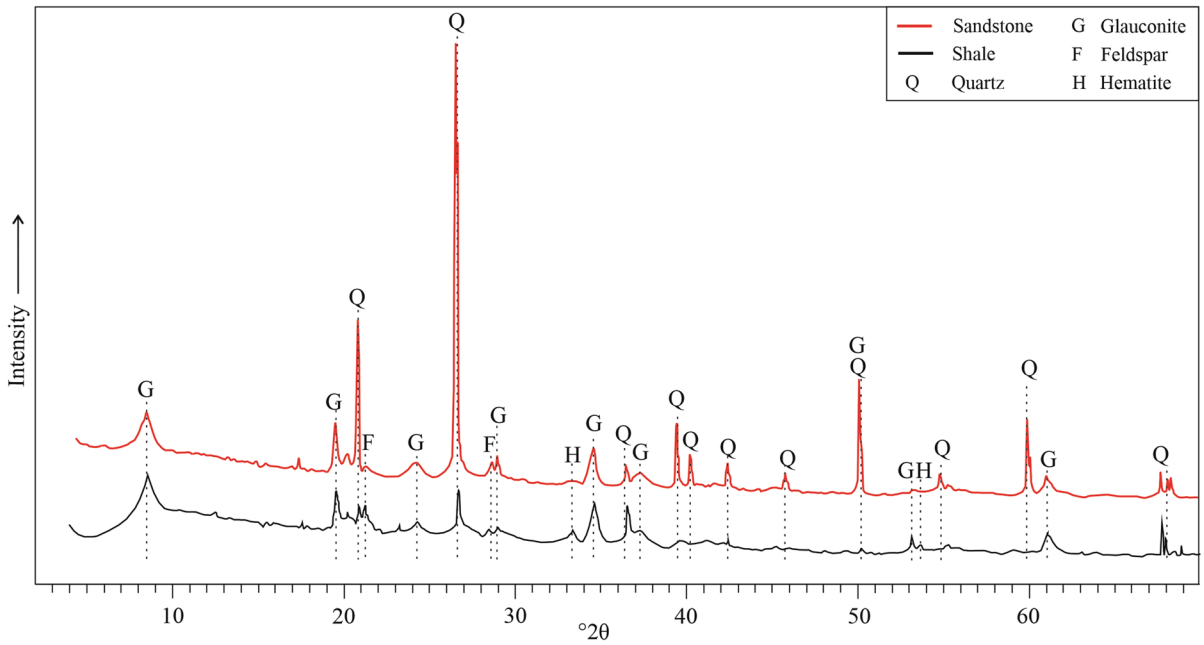

Fig. 5 X-ray diffraction pattern of the bulk glauconitic sandstone and shale of Ukra Member

Major- and trace-element concentrations of glauconite-bearing sandstone and shale are listed in Table 1. The sandstone contains a large proportion of SiO_2 (70.35 wt.%), a moderate amount of Fe_2O_3 (10.75 wt.%), Al_2O_3 (4.41 wt.%), and K_2O (3.93 wt.%), and small amounts of MgO (1.64 wt.%), CaO (0.11 wt.%), Na_2O (0.28 wt.%), and TiO_2 (0.26 wt.%). The glauconitic shale consists of SiO_2 (44.66 wt.%), Fe_2O_3 (31.55 wt.%), K_2O (5.63 wt.%), Al_2O_3 (4.19 wt.%), MgO (1.64 wt.%), Na_2O (0.28 wt.%), TiO_2 (0.26 wt.%), P_2O_5 (0.14 wt.%), and CaO (0.11 wt.%), in decreasing order of their abundance. The sandstone is relatively enriched in SiO_2 (70.35 wt.%) compared to the shale (44.66 wt.%). The large SiO_2 content of sandstone can be attributed to the dominance of quartz in the sample. The shale sample shows an abundance of Fe_2O_3 (31.55 wt.%) which is consistent with the microscopy study. The sandstone and shale samples contain moderate amounts of K_2O i.e. 3.93 and 5.63 wt.%, respectively. The glauconitic sandstone and shale contain trace elements such as Cu, Zn, Mn, Co, Cr, Ni, V, and Mo in considerable amounts. Trace-element analysis of glauconitic sandstone and shale revealed that the concentration of V is greatest, followed by Zn, Cr, Pb, Ni, Mn, Cu, Co, and Mo; the total REE contents are 29.27 ppm and 36.50 ppm, respectively (Table 1).

Mineralogical, Textural, and Chemical Characterization of the Clay Fraction

Mineralogical study of the clay fraction of glauconitic rocks The XRD analysis of the clay fraction (<2 μm) of the glauconite-bearing rock samples was carried out using oriented mounts. The sandstone's glauconite is characterized by a basal diffraction peak at 10.26 Å (001), and non-basal diffraction peaks at 4.98 Å (002), 3.32 Å (003), and, 4.55 Å (020) (Fig. 6). The (112) and (11$\bar{2}$) diffractions were absent from glauconite associated with sandstone indicating that the glauconite is slightly disordered (Thompson & Hower, 1975). The basal (001) diffraction (10.26 Å) was shifted to 9.99 Å upon EG treatment, which indicated the presence of expandable (smectitic) layers in glauconite. The appearance of a narrow, sharp, and symmetrical peak at (001) after heating is further support for the presence of expandable smectitic layers in the glauconite. The AD sample showed an additional diffraction at 12.46 Å, shifted to 16.98 Å after the EG treatment, suggesting the presence of discrete smectite or illite-smectite (López-Quirós et al., 2020). The d_{001} value (10.86 Å) calculated based on the distance between the (001) and (020) peaks indicated

https://doi.org/10.1007/s42860-021-00171-4 Published online by Cambridge University Press

Table 1 Chemical compositions of the glauconitic rocks of Ukra Member of the Bhuj Formation, Gujarat, and and permissible levels of heavy metals in soils, based on Indian standards (Bhatnagar & Awasthi, 2000)

	Glauconitic Sandstone	Glauconitic Shale	Indian Standard (ppm)
Major oxide (wt.%)			
SiO_2	70.35	44.66	
Al_2O_3	4.41	4.19	
Fe_2O_3	10.75	31.55	
K_2O	3.93	5.63	
MgO	1.64	2.78	
CaO	0.11	1.14	
Na_2O	0.28	1.93	
TiO_2	0.26	0.41	
P_2O_5	0.14	0.12	
LOI	5.60	6.78	
Trace elements (ppm)			
V	302.20	286.98	
Cr	183.48	106.09	
As	0.03	0.04	0.05
Sc	8.31	9.75	
Co	2.39	5.50	60–110
Ni	12.78	32.85	75–150
Cu	8.54	8.74	135–270
Zn	77.83	285.61	300–600
Mn	10.21	12.64	
Mo	1.84	2.04	
La	6.71	7.03	
Ce	14.14	14.75	
Pr	1.27	1.86	
Nd	4.49	7.22	
Sm	0.83	1.50	
Eu	0.13	0.28	
Gd	0.50	0.96	
Tb	0.07	0.17	
Dy	0.42	1.07	
Ho	0.07	0.20	
Er	0.21	0.56	
Tm	0.03	0.09	
Yb	0.28	0.66	
Lu	0.04	0.10	
Pb	14.78	34.56	250–500
Th	6.67	8.19	
U	1.73	2.80	
ΣREE	29.27	36.50	

the highly evolved nature of the glauconite (Amorosi et al., 2007).

The AD sample of glauconite present in the shale, exhibited a broadened basal diffraction (001) at 10.18 Å, and other diffractions at 4.56 Å (020), 3.32 Å (003), and 2.58 Å (130) (Fig. 7). A poorly developed peak was observed at 3.09 Å ($11\bar{2}$) whereas the (112) diffraction was absent from the XRD pattern of the shale sample. The oriented XRD pattern treated by EG shows a slight shift of broadened basal diffraction at 9.98 Å of an asymmetrical shape, with incorporated, poorly developed feature at 10.61 Å (Fig. 7). Two diffractions at 9.98 and 10.61 Å after EG treatment indicate that glauconite contains expandable (smectitic) layers (López-Quirós et al., 2020). No diffraction was detected at lower angles than the glauconite's basal diffraction, which indicated the absence of discrete smectite in the shale sample (López-Quirós et al., 2020). On the other hand, a sharp and intense diffraction with a narrow base appeared at 10.14 Å on heating at 550°C. The distance between the (001) and (020) peaks (d_{001} = 10.76) indicated the evolved nature of the glauconite present in the shale (Amorosi et al., 2007).

The near symmetrical basal diffraction (001) and the poorly developed and/or absence of peaks at (112) and ($11\bar{2}$) in the sandstone and shale indicated slight disordering in the structure (Bentor & Kastner, 1965). Such disordered glauconites generally contain 10–20% expandable layers (Bentor & Kastner, 1965; Hower, 1961; Odin & Matter, 1981). A weak response to glycolation was observed in both samples, which indicated that the glauconite contained nearly 10% expandable layers (López-Quirós et al., 2020). The d_{001} value of glauconite present in sandstone and shale indicated a 'highly evolved to evolved' nature of glauconite (Amorosi et al., 2007).

Major-element composition and structural formula of glauconite The major-element composition of glauconites present in sandstone and shale was obtained using EPMA. The micrograph of the glauconitic sandstone is represented in Fig. 8a. The BSE image shows different textures for the different minerals present in the sample. Based on the texture of minerals, a specific location for point EDX over the thin section was selected for analysis. In the sandstone sample, two points for each

https://doi.org/10.1007/s42860-021-00171-4 Published online by Cambridge University Press

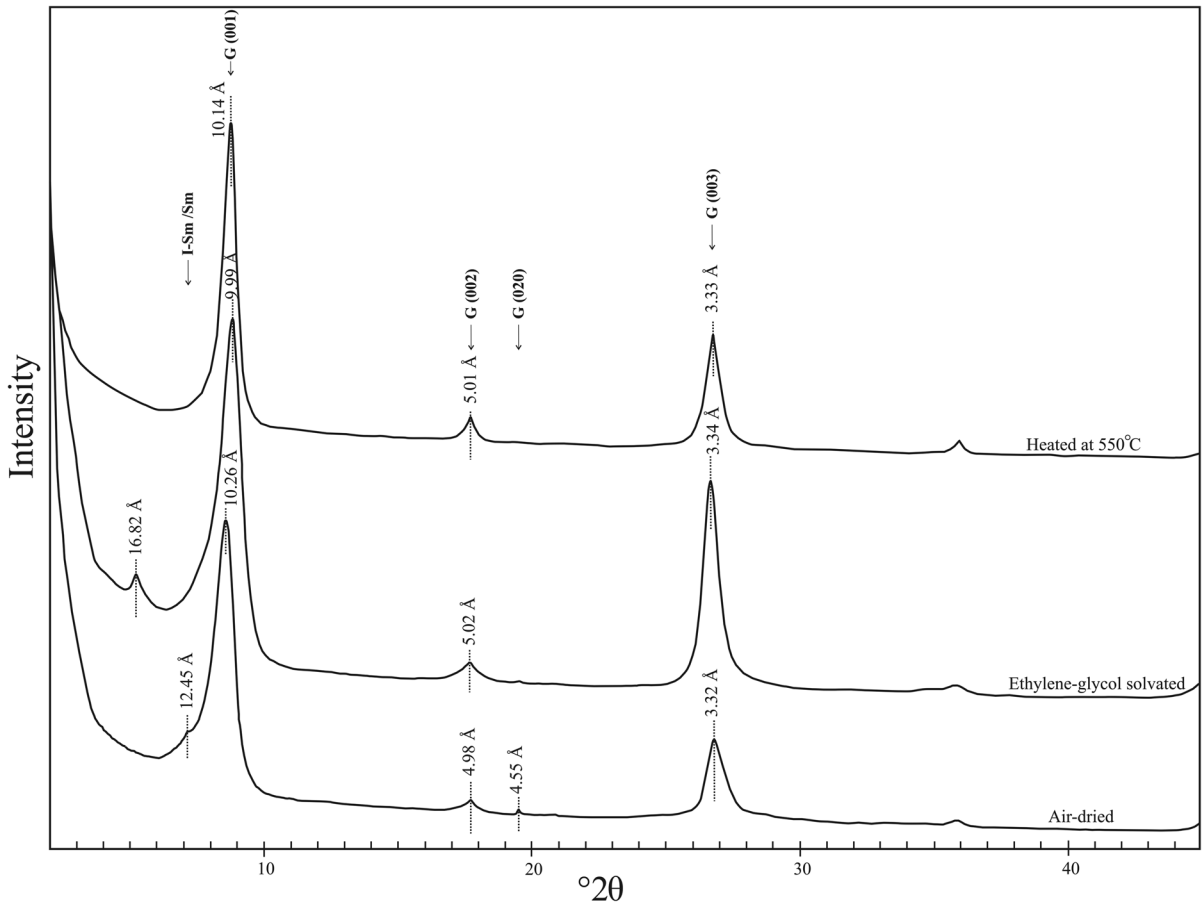

Fig. 6 XRD patterns of an oriented mount of clay separated from sandstone in air-dried state, after glycolation, and after heating at 550°C. The peak shift can be observed upon glycolation and heating. Abbreviations are as follows: G = Glauconite, Sm = Smectite, I-Sm = mixed-layer Illite-Smectite

mineral category were analyzed by EDX (Fig. 8b). The location points 001 and 002 were selected for quartz and 003 and 004 for glauconite. The EDX at points 001 and 002 showed that Si and O are the main elements whereas the other two points (003 and 004) show Si, O, Fe, K, Al, Mg, Ca, Na, and Ti to be major elements (Fig. 8b). The first two points correspond to quartz and the other two points present in the BSE image were identified as glauconite based on their chemical compositions.

Similarly, two points for quartz and two points for glauconite were identified from a thin section of shale (Fig. 8c). The EDX analysis at points 001 and 002 confirmed the presence of quartz (only Si and O are major elements) whereas the other two points 003 and 004 showed Si, Fe, K, Al, Mg, Ca, and Na as characteristic major elements for glauconite (Fig. 8d). The elemental weight was converted to oxide percent. The K_2O content of glauconite present in sandstone was 8.4 wt.%, whereas the glauconite in shale contained 7.4 wt.% of K_2O. The total Fe_2O_3 content was high for both samples. The estimated Fe_2O_3 content of glauconite in the sandstone was 26.2 and 27.13 wt.% in the shale. The Al_2O_3 content was slightly lower (6.94 wt.%) in the sandstone glauconite than in the shale (7.32 wt.%). The SiO_2 content was almost the same in both samples, i.e. 50.08 and 50.30 wt.%, respectively. The MgO content was also similar for glauconites present in both types of rock (Fig. 8b, d). The concentration of CaO and Na_2O in both varieties of glauconite was <1 wt.%.

Based on the potassium oxide and aluminum oxide contents, glauconite maturation was divided into four

https://doi.org/10.1007/s42860-021-00171-4 Published online by Cambridge University Press

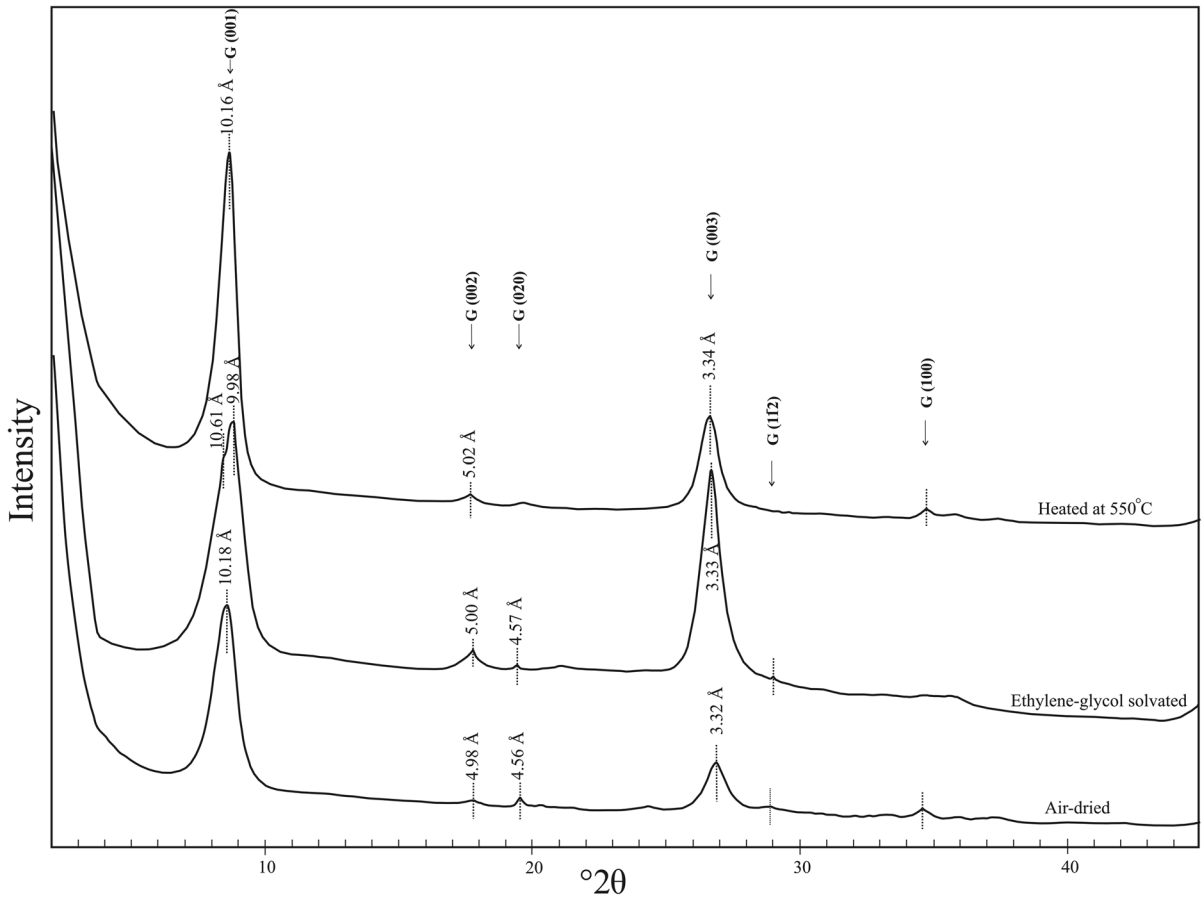

Fig. 7 XRD pattern of an oriented mount of clay separated from shale in air-dried state, after glycolation, and after heating at 550°C. The peak shift can be observed upon glycolation and heating. Abbreviations are as follows: G = Glauconite, Sm = Smectite, I-Sm = mixed-layer Illite-Smectite

stages: (1) nascent stage (2–4 wt.% K_2O; 20–16 wt.% Al_2O_3); (2) slightly evolved stage (4–6 wt.% K_2O; 16–11 wt.% Al_2O_3); (3) evolved stage (6–8 wt.% K_2O; 11–7 wt.% Al_2O_3); and (4) highly evolved stage (>8 wt.% K_2O; <7 wt.% Al_2O_3) (Odin & Matter, 1981). The maturation of glauconite increased with increase in the concentration of potassium with a simultaneous decrease in aluminum content (Odin & Matter, 1981). The K_2O and Al_2O_3 contents of the glauconite concentrate suggested that the glauconite in sandstone belongs to the highly evolved category, whereas the glauconite present in shale had an evolved nature. The residence time of evolved glauconite is 10^4–10^5 years and 10^5–10^6 years for the highly evolved type (Harding et al., 2014; López-Quirós et al., 2020; Odin, 1988).

The stoichiometric formula calculation for both types of glauconite (sandstone and shale) was carried out based on 22 anionic charges per half unit cell. The oxide percent required for calculation was based on the chemical analysis of point 003 of Fig. 8b and d, and gave the chemical formulae $(K_{0.77}\ Na_{0.04}\ Ca_{0.01})_{0.83}\ (Fe_{1.42}\ Ti_{0.01}\ Mg_{0.32}\ Al_{0.20})_{1.95}\ (Si_{3.61}\ Al_{0.38})_4\ O_{10}(OH)_2 \cdot nH_2O$ and $(K_{0.67}\ Na_{0.01}\ Ca_{0.01})_{0.71}\ (Fe_{1.46}\ Mg_{0.31}\ Al_{0.22})_{1.99}\ (Si_{3.60}\ Al_{0.39})_4\ O_{10}\ (OH)_2 \cdot nH_2O$ for the glauconite present in sandstone and shale, respectively. The total iron (Fe) was the dominant octahedral cation with the value of 1.42 and 1.46 apfu for glauconite present in sandstone and shale, respectively. The other octahedral cations, Mg^{2+} and Al^{3+}, were 0.32 and 0.20 apfu, respectively, in the sandstone glauconite, whereas these values were 0.31 and 0.22 apfu, respectively, in the glauconite of shale sample. The Si^{4+} and Al^{3+} contents in the tetrahedral sites were 3.61 and 0.38 apfu, respectively, in the glauconite

https://doi.org/10.1007/s42860-021-00171-4 Published online by Cambridge University Press

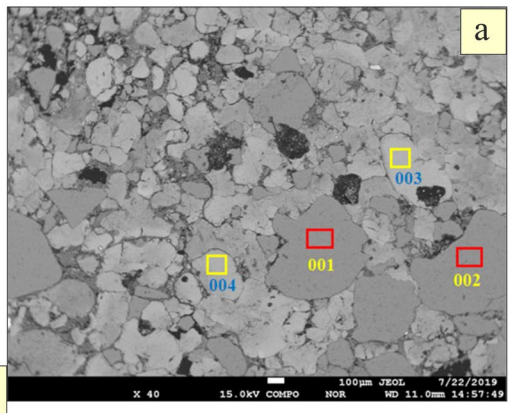

b

Points	Si	O	K	Fe	Al	Mg	Na	Ca	Ti
001	48.58	51.42	-	-	-	-	-	-	-
002	48.30	51.70	-	-	-	-	-	-	-
003	23.04	42.23	6.98	18.08	3.68	1.77	0.24	0.15	0.12
004	23.16	41.28	7.05	17.82	3.75	1.69	0.22	0.13	0.20

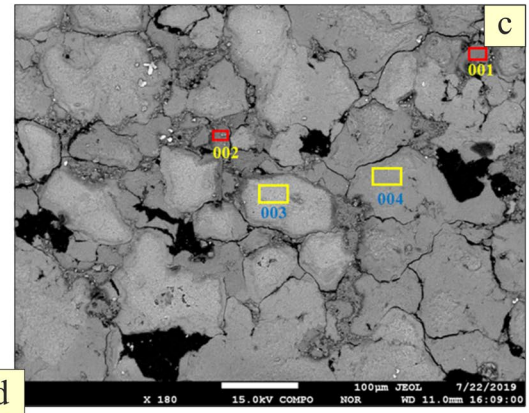

d

Points	Si	O	K	Fe	Al	Mg	Na	Ca
001	46.13	53.87	-	-	-	-	-	-
002	47.44	52.56	-	-	-	-	-	-
003	23.14	43.95	6.15	18.72	3.88	1.73	0.08	0.16
004	23.19	43.89	6.06	18.77	3.92	1.75	0.21	0.37

Fig. 8 **a** EPMA-BSE image of a thin section of a representative glauconitic sandstone and **b** its corresponding EDX chemical analysis at points 001, 002, 003, and 004. **c** EPMA-BSE image of a representative glauconitic shale with **d** its corresponding EDX chemical analysis at points 001, 002, 003, and 004

present in sandstone. In contrast, Si^{4+} and Al^{3+} contents in shale glauconite were 3.60 and 0.39 apfu, respectively. The interlayer K^+ was 0.77 and 0.67 apfu in the sandstone and shale glauconites, respectively. The percentage of non-expandable (glauconite/mica type) and expandable layers present in glauconite was calculated using the interlayer K^+ value (Fernández-Landero & Fernández-Caliani, 2021; López-Quirós et al., 2020), revealing ~91% (9% expandable layers) mica-type layers in glauconite from sandstone and ~85% (15% expandable layers) in shale.

Micro-textural analysis of the clay fractions High-magnification FEG-SEM analysis revealed the morphological features of glauconite present in both types of siliciclastic rocks, i.e. sandstone and shale. Glauconite in sandstone as well as in shale was characterized by well developed 'rosette' or 'flaky honeycomb' structures (Fig. 9a, b). Glauconite present in sandstone exhibits aggregates of curved lamellar glauconite particles ranging in size from 1 to 2 µm. The lamellar structure was a characteristic feature of highly evolved glauconite grains (Fig. 9a). Glauconite present in shale shows irregular flat flakes 0.5–1 µm in size dispersed throughout the matrix, which corroborated the evolved nature of glauconite (Fig. 9b) (Bansal et al., 2017; Wright et al., 1987). Thus, the FEG-SEM analysis was consistent with the maturity evaluation observed in the petrographic, XRD, and EPMA analyses.

Infrared spectra of the clay fractions The FTIR spectra of two clay fractions observed over the range 4000–500 cm^{-1} revealed the existence of five high-frequency absorption bands (Fig. 10). The prominent peak at 3540 cm^{-1} was related to the stretching vibrations of structural hydroxyl groups (–OH), which were attached to Al^{3+}, Mg^{2+}, Fe^{2+}, and/or Fe^{3+} in the octahedral sheet (Odin, 1988; Petit et al., 1999; Selim et al., 2014). The other feature at 1630 cm^{-1} was due to the H–O–H bending vibration present in the interlayer space (Russell et al., 1970). The most intense peak at 960 cm^{-1} was assigned to in-plane Si–O–Si lattice vibrations (Sanchez-Navas et al., 2008; Selim et al., 2018). The other absorption peaks at 812 cm^{-1} and 665 cm^{-1} were attributed to the out-of-plane bending vibration of $Fe^{3+}MgOH/Fe^{3+}Fe^{2+}OH$ and structural vibrations of –OH groups, respectively (Bishop et al., 2008; Haaland et al., 2017). The absorption peak at 960 cm^{-1} for glauconitic sandstone had more band depth due to less substitution of Al^{3+} for Si^{4+} in the tetrahedral structure of glauconite (Chattoraj et al., 2018; Younes et al., 2019). This observation agreed with the EPMA results which

https://doi.org/10.1007/s42860-021-00171-4 Published online by Cambridge University Press

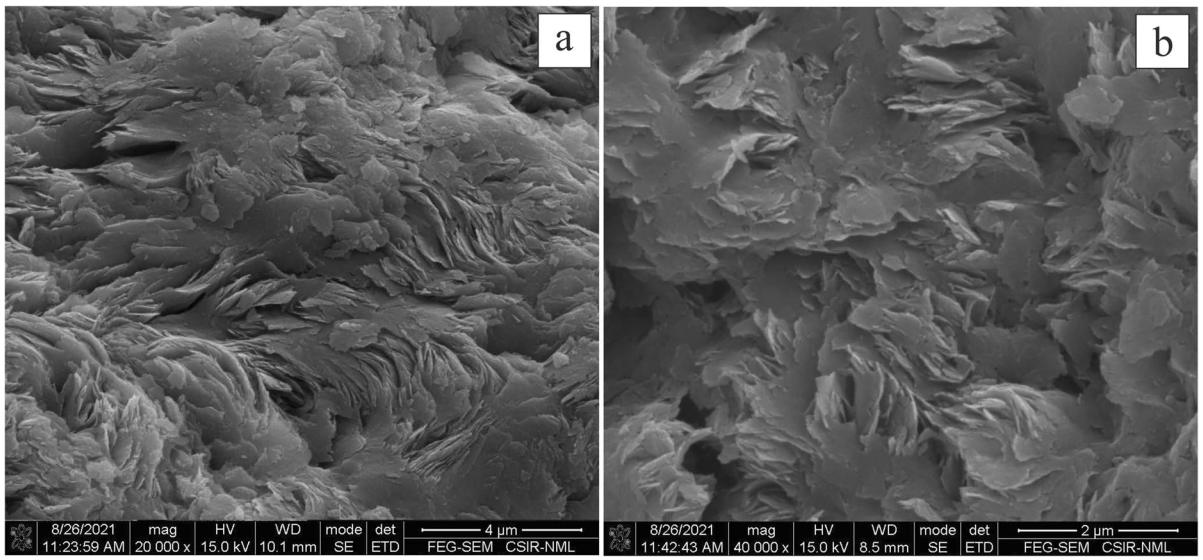

Fig. 9 SEM image showing the internal structure of glauconite from **a** sandstone and **b** shale

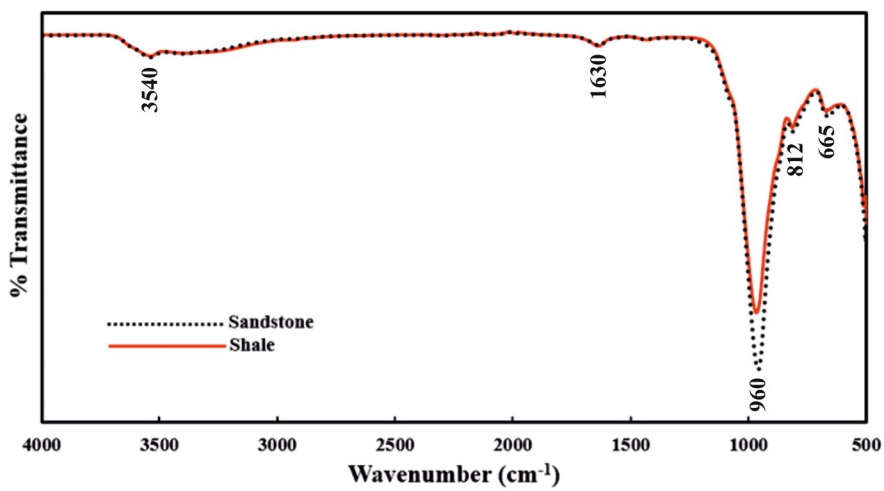

Fig. 10 IR spectra of clay fractions from both the shale and the sandstone

showed that less Al^{3+} had substituted for Si^{4+} in the sandstone glauconite.

Discussion

The integrated mineralogical and geochemical investigations of glauconitic rocks belonging to the Ukra Member (Bhuj Formation) at Kutch highlight an important aspect of glauconite maturation. Glauconite occurs mainly in sandstone and shale horizons of the Ukra Member. The petrographic and bulk XRD analyses indicated that quartz, glauconite, feldspar, and iron oxide are the major mineral constituents of the rock samples. Glauconitic shale contains more glauconite than glauconitic sandstone. The trace-element

https://doi.org/10.1007/s42860-021-00171-4 Published online by Cambridge University Press

study strengthened the interpretation as the observed higher concentration of trace elements (V, Co, Ni, Cu, Zn, Mo, and REE) in shale can be attributed to a large clay content (glauconite). The penetrating fractures in glauconite indicate the in situ formation of glauconite along the cleavage and fracture planes of feldspar grains (Amorosi, 1995; Baldermann et al., 2017; Bansal et al., 2017; Li et al., 2012). The analytical results obtained from XRD and EPMA show that the glauconites present in sandstone and shale are slightly disordered and contain small proportions (9–15%) of interstratified expandable (smectite) layers. The results also showed the glauconites to be mature. The K_2O contents (7.5–8.5%) and d_{001} (10.76–10.86 Å) values for the glauconites of the Ukra Member are comparable with the values proposed by Amorosi et al. (2007) for evolved to highly evolved glauconites. The glauconite associated with sandstone and shale containing high K^+ (0.77 and 0.67 apfu) at interlayer sites also indicated the highly mature stage of glauconite development (Baldermann et al., 2013, 2017). The high degree of maturity was further confirmed by the position of a Si–O absorption band near 1000 cm^{-1} in the FTIR spectra (Li et al., 2012). The autochthonous and highly evolved nature of glauconite suggested a low rate of sedimentation and its formation during transgression (Bansal et al., 2017; Li et al., 2012; López-Quirós et al., 2019).

Glauconitic rocks which contain at least 2.2–4 wt.% K_2O are considered as potential potash fertilizer (Franzosi et al., 2014; Karimi et al., 2012; Rudmin et al., 2017) for countries where conventional sources of potassium are unavailable. Glauconitic rocks containing ~3–6 wt.% K_2O have been beneficiated to enhance their potassium contents (Shekhar et al., 2017a; Shekhar et al., 2017b; Sontakkey et al., 2017) for direct application and conversion into a soluble, commercial fertilizer product (Castro & Tourn, 2003; Mohammed et al., 2014; Rudmin et al., 2019; Shirale et al., 2019). The K_2O content of glauconitic sandstone and shale of the Ukra Member (Bhuj Formation) is 3.93 and 5.63 wt.%, respectively (Table 1). The glauconite fraction associated with the rocks of the Ukra Member contains 7.4–8.4 wt.% K_2O. Moreover, the glauconitic rocks contain micronutrients such as Zn, Mn, Cu, Co, Mo, and Ni, which are beneficial for plant growth (Tripathi et al., 2015) (Table 1). The concentrations of heavy metals present in the glauconitic rocks are less than the permissible levels (Bhatnagar & Awasthi, 2000) and, hence, are not toxic to plant and human health. The glauconitic rocks of the Ukra Formation containing mature glauconite pellets, have large K_2O contents (~4–5.6 wt.%) and essential micronutrients and can, thus, be considered as a source of fertilizer after appropriate beneficiation.

Conclusions

(1) In the present study, the occurrence of glauconite was observed in siliciclastic rocks belonging to the Ukra Member of the Bhuj Formation, which are exposed in the Guneri and Umarsar area of the Kutch District, Gujarat. The host rock for the glauconite in Guneri is sandstone whereas glauconite occurs in shale in the Umarsar area.

(2) The glauconite showed a greenish appearance in sandstone while it was brownish in shale. Glauconite occurred as pellets exhibiting variable external morphologies ranging from ovoid or spheroidal to ellipsoidal in sandstone as well as shale samples. In addition, glauconite showed significant fractures indicating an in situ origin.

(3) Based on the XRD analysis of the clay fraction recovered from the bulk-rock samples, the glauconite in sandstone and shale was identified as being of slightly disordered type with few interstratified expandable layers. The distance between the (001) and (020) XRD peaks (d_{001} = 10.76–10.86 Å) indicated a high degree of maturation of the glauconites associated with sandstone and shale.

(4) The mineral chemistry determined by EPMA showed that the glauconite grains present in sandstone were relatively enriched in K_2O (8.4 wt.%) compared to that of the glauconite in the shale (7.4 wt.%). In both cases, however, the degree of maturity is high. The sandstone contained highly evolved glauconite and the glauconite present in shale was of an evolved nature.

(5) The 'curved lamellar' internal morphology of the glauconite present in sandstone indicated its highly evolved (highly matured) nature. In contrast, the glauconite in shale shows an irregular, flaky structure confirming an evolved (matured) nature.

https://doi.org/10.1007/s42860-021-00171-4 Published online by Cambridge University Press

(6) The highly evolved and autochthonous glauconite, indicating the low rate of sedimentation, must have formed during the period of transgression. The glauconite-bearing siliciclastic rocks (Ukra Member) from the Guneri and Umarsar areas were, therefore, likely to have been deposited during the high stand. This study supports the other sedimentological and paleontological studies which considered the Ukra Member to be a transgressive tongue in the Bhuj Formation of the Kutch Basin.

(7) The glauconitic rocks containing evolved to highly evolved glauconite along with other micronutrients can be considered as a potential alternative source of potash after appropriate physicochemical beneficiation and reserve estimation.

Acknowledgments The authors thank the director, CSIR-National Metallurgical Laboratory, for his permission to publish this paper. This research work was supported and funded by the In-House Research Project (OLP 0294) of the National Metallurgical Laboratory. The authors are grateful to Mr. Hajaj Basheer, Geologist (Sr.) of the Geological Survey of India (GSI), Gujarat, for providing the glauconitic rock samples.

Funding Funding sources are as stated in the Acknowledgments.

Declarations

Conflict of Interest The authors declare that they have no conflict of interest.

References

Amorosi, A. (1995). Glaucony and sequence stratigraphy: A conceptual framework of distribution in siliciclastic sequences. *Journal of Sedimentary Research, 65*, 419–425. https://doi.org/10.1306/D4268275-2B26-11D7-8648000102C1865D

Amorosi, A. (2012). The occurrence of glaucony in the stratigraphic record: distribution patterns and sequence-stratigraphic significance. *International Association of Sedimentologists. Special Publication, 45*, 37–54.

Amorosi, A. (2013). The occurrence of glaucony in the stratigraphic record: distribution patterns and sequence stratigraphic significance. In: Morad, S., Ketzer, M., de Ros, L.F. (Eds.). *Linking Diagenesis to Sequence Stratigraphy, 45*, 37–53. https://doi.org/10.1002/9781118485347.ch2

Amorosi, A., Sammartino, I., & Tateo, F. (2007). Evolution patterns of glaucony maturity: a mineralogical and geochemical approach. *Deep Sea Research Part II: Topical Studies in Oceanography, 54*, 1364–1374.

Bailey, S. W. (1980). Summary of recommendations of AIPEA nomenclature committee. *Clays and Clay Minerals, 28*, 73–78. https://doi.org/10.1346/CCMN.1980.0280114

Baldermann, A., Grathoff, G. H., & Nickel, C. (2012). Micromilieu-controlled glauconitization in fecal pellets at Oker (Central Germany). *Clay Minerals, 47*, 513–538. https://doi.org/10.1180/claymin.2012.047.4.09

Baldermann, A., Warr, L. N., Grathoff, G. H., & Dietzel, M. (2013). The rate and mechanism of deep-sea glauconite formation at the Ivory Coast-Ghana marginal ridge. *Clays and Clay Minerals, 61*, 258–276. https://doi.org/10.1346/CCMN.2013.0610307

Baldermann, A., Dietzel, M., Mavromatis, V., Mittermayr, F., Warr, L. N., & Wemmer, K. (2017). The role of Fe on the formation and diagenesis of interstratified glauconite-smectite and illite-smectite: a case study of Upper Cretaceous shallow-water carbonates. *Chemical Geology, 453*, 21–34. https://doi.org/10.1016/j.chemgeo.2017.02.008

Banerjee, S., Kumar, S. J., & Eriksson, P. G. (2008). Mg-rich ferric illite in marine transgressive and high stand system tracts: examples from the Palaeoproterozoic Semri Group, central India. *Precambrian Research, 162*, 212–226. https://doi.org/10.1016/j.precamres.2007.07.018

Banerjee, S., Chattoraj, S. L., Saraswati, P. K., Dasgupta, S., & Sarkar, U. (2012a). Substrate control on formation and maturation of glauconites in the Middle Eocene Harudi Formation, western Kutch, India. *Marine and Petroleum Geology, 30*, 144–160. https://doi.org/10.1016/j.marpetgeo.2011.10.008

Banerjee, S., Chattoraj, S. L., Saraswati, P. K., Dasgupta, S., Sarkar, U., & Bumby, A. (2012b). The origin and maturation of lagoonal glauconites: a case study from the Oligocene Maniyara Fort Formation, western Kutch. *Journal of the Geological Society of India, 47*, 357–371. https://doi.org/10.1002/gj.1345

Banerjee, S., Mondal, S., Chakraborty, P. P., & Meena, S. S. (2015). Distinctive compositional characteristics and evolutionary trend of Precambrian glaucony: Example from Bhalukona Formation, Chhattisgarh basin, India. *Precambrian Research, 271*, 33–48. https://doi.org/10.1016/j.precamres.2015.09.026

Banerjee, S., Bansal, U., Pande, K., & Meena, S. S. (2016a). Compositional variability of glauconites within the Upper Cretaceous Karai Shale Formation, Cauvery Basin, India: Implications for evaluation of stratigraphic condensation. *Sedimentary Geology, 331*, 12–29. https://doi.org/10.1016/j.sedgeo.2015.10.012

Banerjee, S., Bansal, U., & Thorat, A. (2016b). A review on palaeogeographic implications and temporal variation in glaucony composition. *Palaeogeography, Palaeoclimatology, Palaeoecology, 5*, 43–71. https://doi.org/10.1016/j.jop.2015.12.001

Banerjee, S., Farouk, S., Nagm, E., Choudhury, T. R., & Meena, S. S. (2019). High Mg-glauconite in the Campanian Duwi Formation of Abu Tartur Plateau, Egypt and its implications. *Journal of African Earth Sciences, 156*, 12–25. https://doi.org/10.1016/j.jafrearsci.2019.05.001

Bansal, U., Banerjee, S., Pande, K., Arora, A., & Meena, S. S. (2017). The distinctive compositional evolution of glauconite in the Cretaceous Ukra Hill Member (Kutch basin, India) and its implications. *Marine and Petroleum Geology, 82*, 97–117. https://doi.org/10.1016/j.marpetgeo.2017.01.017

Bansal, U., Banerjee, S., Ruidas, D. K., & Pande, K. (2018). Origin and geochemical characterization of Maastrichtian glauconites in the Lameta Formation, Central India. *Palaeogeography, Palaeoclimatology, Palaeoecology, 7*, 99–116. https://doi.org/10.1016/j.jop.2017.12.001

Bansal, U., Banerjee, S., & Nagendra, R. (2020). Is the rarity of glauconite in Precambrian Bhima Basin in India related to its chloritization? *Precambrian Research, 336*, 105509. https://doi.org/10.1016/j.precamres.2019.105509

Bentor, Y. K., & Kastner, M. (1965). Notes on the mineralogy and origin of glauconite. *Journal of Sedimentary Petrology, 35*, 155–166. https://doi.org/10.1306/74D71212-2B21-11D7-8648000102C1865D

Bhatnagar, J. P., & Awasthi, S. K. (2000). *Prevention of food adulteration act (act no. 37 of 1954) along with central & state rules (as amended for 1999)*. Ashoka Law House.

Bishop, J. L., Lane, M. D., Dyar, M. D., & Brown, A. J. (2008). Reflectance and emission spectroscopy study of four groups of phyllosilicates: smectites, kaolinite, serpentines, chlorites and micas. *Clay Minerals, 43*, 35–54. https://doi.org/10.1180/claymin.2008.043.1.03

Biswas, S. K. (1977). Mesozoic rock-stratigraphy of Kutch, Gujarat. *Quarterly Journal of the Geological Mineralogical and Metallurgical Society of India, 49*, 1–51. https://doi.org/10.17491/cgsi/2016/105405

Biswas, S. K. (1987). Regional tectonic framework, structure and evolution of the western marginal basins of India. *Tectonophysics, 135*, 307–327. https://doi.org/10.1016/0040-1951(87)90115-6

Biswas, S. K. (2005). A review of structure and tectonics of Kutch basin, western India, with special reference to earthquakes. *Current Science, 88*, 1592–1600.

Burst, J. F. (1958). Mineral heterogeneity in glauconite pellets. *American Mineralogist, 43*, 481–497.

Castro, L., & Tourn, S. (2003). Direct application of phosphate rocks and glauconite as alternative sources of fertilizer in Argentina. *Exploration and Mining Geology, 12*, 71–78.

Chamley, H. (1989). *Clay Sedimentology*. Springer-Verlag. https://doi.org/10.1007/978-3-642-85916-8

Chattoraj, S. L., Banerjee, S., & Saraswati, P. K. (2009). Glauconites from the Late Palaeocene-Early Eocene Naredi Formation, western Kutch and their genetic implications. *Journal of the Geological Society of India, 73*, 567–574. https://doi.org/10.1007/s12594-009-0040-x

Chattoraj, S. L., Banerjee, S., Meer, F. V. D., & Ray, P. K. C. (2018). Application of visible and infrared spectroscopy for the evaluation of evolved glauconite. *International Journal of Applied Earth Observation and Geoinformation, 64*, 301–310. https://doi.org/10.1016/j.jag.2017.02.007

Choudhuri, R., Balagopal, A. T., & Banerjee, K. C. (1973). Availability of potash from non-traditional sources. *Technology., 10*, 128–131.

Dasgupta, S., Cahudhuri, A. K., & Fukuoka, M. (1990). Compositional characteristics of glauconitic alterations of K-feldspar from India and their implications. *Journal of Sedimentary Petrology, 60*, 277–281.

Desai, B. G. (2013). Iconological analysis of transgressive marine tongue in prograding deltaic system: Evidences from Ukra Hill Member, Western Kachchh, India. *Journal of the Geological Society of India, 82*, 143–152. https://doi.org/10.1007/s12594-013-0132-5

Desai, B. G., & Saklani, R. D. (2012). Significance of the trace fossil Balanoglossites Mägdefrau, 1932 from the Lower Cretaceous Guneri member (Bhuj formation) of the Guneri dome, Kachchh, India. *Swiss Journal of Palaeontology, 131*, 255–263. https://doi.org/10.1007/s13358-012-0045-8

Dooley, J. H. (2006). Glauconite. In J. Koger, N. Trivedi, J. Barrer, & N. Krukowsky (Eds.), *Industrial Minerals and Rocks* (pp. 495–506). SME.

Drits, V. A., Ivanovskaya, T. A., Sakharov, B. A., Zvyagina, B. B., Derkowski, A., Gor'kova, N. V., Pokrovskaya, E. V., Savichev, A. T., & Zaitseva, T. S. (2010). Nature of the structural and crystal chemical heterogeneity of the Mg–rich glauconite (Riphean, Anabar Uplift). *Lithology and Mineral Resources, 45,* 555–576. https://doi.org/10.1134/S0024490210060040.

El-Habaak, G., Askalany, M., Faraghaly, M., & Abdel-Hakeem, M. (2016). The economic potential of El-Gedida glauconite deposits, El-Bahariya Oasis, Western Desert, Egypt. *Journal of African Earth Sciences, 120*, 186–197. https://doi.org/10.1016/j.jafrearsci.2016.05.007

Essa, M. A., Ahmed, E. A., & Kurzweil, H. (2016). Genesis, maturity and weathering of some Upper Cretaceous Egyptian glauconites: mineralogical and geochemical implications. *Journal of African Earth Sciences, 124*, 427–446. https://doi.org/10.1016/j.jafrearsci.2016.09.036

Fernández-Landero, S., & Fernández-Caliani, J. C. (2021). Mineralogical and Crystal-Chemical Constraints on the Glauconite-Forming Process in Neogene Sediments of the Lower Guadalquivir Basin (SW Spain). *Minerals, 11*, 578.

Franzosi, C., Castro, L. N., & Celeda, A. M. (2014). Technical evaluation of glauconies as alternative potassium fertilizer from the Salamanca Formation, Patagonia, Southwest Argentina. *Natural Resources Research, 23*, 311–320. https://doi.org/10.1007/s11053-014-9232-1

Fürsich, F. T., & Pandey, D. K. (2003). Sequence stratigraphic significance of sedimentary cycles and shell concentrations in the Upper Jurassic–Lower Cretaceous of Kachchh, western India. *Palaeogeography, Palaeoclimatology, Palaeoecology, 193*, 285–309. https://doi.org/10.1016/S0031-0182(03)00233-5

Haaland, M. M., Friesem, D. E., Miller, C. E., & Henshilwood, C. S. (2017). Heat-induced alteration of glauconitic minerals in the Middle Stone Age levels of Blombos Cave, South Africa: implications for evaluating site structure and burning events. *Journal of Archaeological Science, 86*, 81–100. https://doi.org/10.1016/j.jas.2017.06.008

Harder, H. (1980). Syntheses of glauconite at surface temperatures. *Clays and Clay Minerals, 28*, 217–222. https://doi.org/10.1346/CCMN.1980.0280308

Harding, S. C., Nash, B. P., Petersen, E. U., Ekdale, A. A., Bradbury, C. D., & Dyar, M. D. (2014). Mineralogy and

geochemistry of the main glauconite bed in the middle Eocene of Texas: Paleoenvironmental Implications for the Verdine Facies. *PLoS One, 9*, e87656. https://doi.org/10.1371/journal.pone.0087656

Hassan, M. S., & Baioumy, H. M. (2006). Structural and chemical alteration of glauconite under progressive acid treatment. *Clays and Clay Minerals, 54*, 491–499. https://doi.org/10.1346/CCMN.2006.0540410

Hower, J. (1961). Some factors concerning the nature and origin of glauconite. *American Mineralogist, 46*, 313–334.

Huggett, J. M., & Gale, A. S. (1997). Petrology and palaeoenvironmental significance of glaucony in the Eocene succession at Whitecliff Bay, Hampshire Basin, UK. *Journal of the Geological Society, 154*, 897–912. https://doi.org/10.1144/gsjgs.154.5.0897

Innes, R. P., & Pluth, D. J. (1970). Thin Section Preparation Using an Epoxy Impregnation for Petrographic and Electron Microprobe Analysis 1. *Soil Science Society of America Journal, 34*, 483–485. https://doi.org/10.2136/sssaj1970.03615995003400030035x

Jackson, M. L. (1979). *Soil chemical analysis – advanced course* (2nd edn.). 11th printing, Madison, Wisconsin, pp. 169–251.

Jain, R. L. (1997). *Study of search of potash in glauconite bearing shale and sandstone in kachchh District, Gujarat* (pp. 1994–1995). Geological Survey of India, progress report for the FSP.

Janardhana Rao, L. H., Srinivasarao, C., & Ramakrishnan, T. L. (1975). Reclassification of the rocks of Bhima basin, Gulburga district, Mysore state. *Geological Survey of India, Miscellaneous Publication, 23*, 177–184.

Karimi, E., Abdolzadeh, A., Sadeghipour, H. R., & Aminei, A. (2012). The potential of glauconitic sandstone as a potassium fertilizer for olive plants. *Archives of Agronomy and Soil Science, 58*, 983–993. https://doi.org/10.1080/03650340.2011.557369

Kelly, J. C., & Webb, J. A. (1999). The genesis of glaucony in the Oligo-Miocene Torquay Group, south eastern Australia: petrographic and geochemical evidence. *Sedimentary Geology, 125*, 99–114. https://doi.org/10.1016/S0037-0738(98)00149-3

Kübler, B. (1983). Dosage quantitatif des minéraux majeurs des roches sédimentaires par diffraction X. *Cahiers de l'Institut de Géologie Series AX, 1*(1), 1–13.

Kumar, V., & Bakliwal, P. C. (2005). Potash in India. *Geological Survey of India. Miscellaneous. Publication, 65*, xiii, 134.

Kuran, B., & Sahiwala, N. K. (1999). Study for search for potash in Glauconite-bearing shale and sandstone, Gujarat. *Record of Geological Survey of India, 129*, 48–49.

Li, X., Cai, Y., Hu, X., Huang, Z., Wang, J., & Christidis, G. (2012). Mineralogical characteristics and geological significance of Albian (Early Cretaceous) glauconite in Zanda, southwestern Tibet, China. *Clay Minerals, 47*, 45–58. https://doi.org/10.1180/claymin.2012.047.1.45

López-Quirós, A., Escutia, C., Sánchez-Navas, A., Nieto, F., Garcia-Casco, A., Martín-Algarra, A., Evangelinos, D., & Salabarnada, A. (2019). Glaucony authigenesis, maturity and alteration in the Weddell Sea: An indicator of paleoenvironmental conditions before the onset of Antarctic glaciation. *Scientific Reports, 9*, 13580–13592. https://doi.org/10.1038/s41598-019-50107-1

López-Quirós, A., Sánchez-Navas, A., Nieto, F., & Escutia, C. (2020). New insights into the nature of glauconite. *American Mineralogist: Journal of Earth and Planetary Materials, 105*, 674–686.

Mandal, S., Banerjee, S., Sarkara, S., Mondal, I., & Choudhury, T. R. (2020). Origin and sequence stratigraphic implications of high-alumina glauconite within the Lower Quartzite, Vindhyan Supergroup. *Marine and Petroleum Geology, 112*, 104040–104055. https://doi.org/10.1016/j.marpetgeo.2019.104040

Manghnani, M. H., & Hower, J. (1964a). Glauconites: cation exchange capacities and infrared spectra. Part I: The cation exchange capacity of glauconite. *American Mineralogist, 49*, 586–598.

Manghnani, M. H., & Hower, J. (1964b). Glauconites: cation exchange capacities and infrared spectra. Part II:Infrared absorption characteristics of glauconites. *American Mineralogist, 49*, 1631–1642.

McRae, S. G. (1972). Glauconite. *Earth-Science Reviews, 8*, 397–440. https://doi.org/10.1016/0012-8252(72)90063-3

Mishra, R. N., Jayaprakash, A. V., Hans, S. K., & Sundaram, V. (1987). Bhima Group of Upper Proterozoic–a Stratigraphic puzzle. *Memoirs–Geological Society of India, 6*, 227–237.

Mohammed, S. M. O., Brandt, K., Gray, N. D., White, M. L., & Manning, D. A. C. (2014). Comparison of silicate minerals as sources of potassium for plant nutrition in sandy soil. *European Journal of Soil Science, 65*, 653–662. https://doi.org/10.1111/ejss.12172

Odin, G. S. (1988). Green marine clays. Oolitic ironstone facies, verdine facies, glaucony facies and celadonite-bearing facies — A comparative study. *Developments in Sedimentology, 45*, Elsevier Science Publishers, Amsterdam. https://doi.org/10.1180/claymin.1989.024.3.11

Odin, G. S., & Matter, A. (1981). De glauconiarum origine. *Sedimentology, 28*, 611–641. https://doi.org/10.1111/j.1365-3091.1981.tb01925.x

Paul, D. K., Ray, A., Das, B., Patil, S. K., & Biswas, S. K. (2008). Petrology, geochemistry and paleomagnetism of the earliest magmatic rocks of Deccan Volcanic Province, Kutch, Northwest India. *Lithos, 102*, 237–259. https://doi.org/10.1016/j.lithos.2007.08.005

Petit, S., Madejová, J., Decarreau, A., & Martin, F. (1999). Characterization of octahedral substitutions in kaolinites using near-infrared spectroscopy. *Clays and Clay Minerals, 47*, 103–108. https://doi.org/10.1346/CCMN.1999.0470111

Rahimzadeh, N., Khormali, F., Olamaee, M., Amini, A., & Dordipour, E. (2015). Effect of canola rhizosphere and silicate dissolving bacteria on the weathering and K release from indigenous glauconite shale. *Biology and Fertility of Soils, 51*, 973–981. https://doi.org/10.1007/s00374-015-1043-y

Rawlley, R. K. (1994). Mineralogical investigations on an Indian glauconitic sandstone of Madhya Pradesh state. *Applied Clay Science, 8*, 449–465. https://doi.org/10.1016/0169-1317(94)90039-6

Rieder, M., Cavazzini, G., Dyakonov, Y. S., Frank-Kamenetskii, V. A., Gottardi, G., Guggenheim, S., Koval, P. V., Müller, G., Neiva, A. M. R., Radoslovich, E. W., Roberts, J. L., Sassi, F. P., Takeda, H., Weiss, Z., & Wones, D. R. (1998). Nomenclature of the micas. *Clays and Clay Minerals, 46*, 586–595. https://doi.org/10.1346/CCMN.1998.0460513

Rudmin, M., Banerjee, S., Mazurov, A., Makarov, B., & Martemyanov, D. (2017). Economic potential of glauconitic rocks in Bakchar deposit (S-E Western Siberia) for alternate potash fertilizer. *Applied Clay Science, 150*, 225–233. https://doi.org/10.1016/j.clay.2017.09.035

Rudmin, M., Banerjee, S., Makarov, B., Mazurov, A., Ruban, A., Oskina, Y., Tolkachev, O., Buyakov, A., & Shaldybin, M. (2019). An investigation of plant growth by the addition of glauconitic fertilizer. *Applied Clay Science, 180*, 105178–105186. https://doi.org/10.1016/j.clay.2019.105178

Russell, J. D., Farmer, V. C., & Velde, B. (1970). Replacement of OH by OD in layer silicates, and identification of the vibrations of these groups in infra-red spectra. *Mineralogical Magazine, 37*, 869–879. https://doi.org/10.1180/minmag.1970.037.292.01

Sanchez-Navas, A., Martín-Algarra, A., Eder, V., Reddy, B. J., Nieto, F., & Zanin, Y. N. (2008). Color, mineralogy and composition of upper Jurassic west Siberian glauconite: useful indicators of paleoenvironment. *Canadian Mineralogist, 46*, 1545–1564. https://doi.org/10.3749/canmin.46.5.1249

Schimicoscki, R. S., Oliveira, K. D., & Avila-Neto, C. N. (2020). Potassium recovery from a Brazilian glauconite siltstone via reaction with sulphuric acid in hydrothermal conditions. *Hydrometallurgy, 191*, 105251–105259. https://doi.org/10.1016/j.hydromet.2020.105251

Selim, K. A., Youssef, M. A., Abd El-Rahiem, F. H., & Hassan, M. S. (2014). Dye removal using some surface modified silicate minerals. *International Journal of Mining Science and Technology, 24*, 183–189. https://doi.org/10.1016/j.ijmst.2014.01.007

Selim, K. A., El-Tawil, R. S., & Rostom, M. (2018). Utilization of surface modified phyllosilicate mineral for heavy metals removal from aqueous solutions. *Egyptian Journal of Petroleum, 27*, 393–401. https://doi.org/10.1016/j.ejpe.2017.07.003

Shekhar, S., Mishra, D., Agrawal, A., & Sahu, K. K. (2017a). Physical and chemical characterization and recovery of potash fertilizer from glauconitic clay for agricultural application. *Applied Clay Science, 143*, 50–56. https://doi.org/10.1016/j.clay.2017.03.016

Shekhar, S., Mishra, D., Agrawal, A., & Sahu, & K. K. (2017b). Physico-chemical treatment of glauconitic sandstone to recover potash and magnetite. *Journal of Cleaner Production, 147*, 681–693. https://doi.org/10.1016/j.jclepro.2017.01.127

Shekhar, S., Sinha, S., Mishra, D., Agrawal, A., & Sahu, K. K. (2020). A sustainable process for the recovery of potash fertilizer from glauconite through simultaneous production of pigment grade red oxide. *Sustainable Materials and Technology, 23*, e00129–e00137. https://doi.org/10.1016/j.susmat.2019.e00129

Shirale, A. O., Meena, B. P., Gurav, P. P., Srivastava, S., Biswas, A. K., Thakur, J. K., Somasundaram, J., Patra, A. K., & Rao, A. S. (2019). Prospects and challenges in utilization of indigenous rocks and minerals as source of potassium in farming rocks and minerals as source of potassium. *Journal of Plant Nutrition, 42*, 2682–2701. https://doi.org/10.1080/01904167.2019.1659353

Soni, M. K. (1990). On the possibility of using glauconite sandstone as a source of raw material for potash fertilizer. *Mining and Engineering Journal, 1,* 3–10.

Sontakkey, V.A., Aehdi, R.S., Mohanram, I., Aruna, V.A.J., Lal, S.M., & Ravindran, I., (2017). Beneficiation of a glauconite sandstone sample, Kurchha-Barwadih area, Sonbhadra District, Uttar Pradesh. In: *International Seminar on Mineral Processing Technology (MPT-XVI), Chennai*, 1–3 February, 2017.

Soukup, D. A., Buck, B. J., & Harris, W. (2008). Preparing soils for mineralogical analyses. Methods of Soil Analysis Part 5- Mineralogical. *Methods, 5*, 13–31. https://doi.org/10.2136/sssabookser5.5.c2

Srasra, E., & Trabelsi-Ayedi, M. (2000). Textural properties of acid-activated glauconite. *Applied Clay Science, 17*, 71–84. https://doi.org/10.1016/S0169-1317(00)00008-9

Stille, P., & Clauer, N. (1994). The process of glauconitization: chemical and isotopic evidence. *Contributions to Mineralogy and Petrology, 117*, 253–262. https://doi.org/10.1007/BF00310867

Tang, D., Shi, X., Jiang, G., Zhou, X., & Shi, Q. (2017a). Ferruginous seawater facilitates the transformation of glauconite to chamosite: An example from the Mesoproterozoic Xiamaling Formation of North China. *American Mineralogist, 102*, 2317–2332. https://doi.org/10.2138/am-2017-6136

Tang, D. J., Shi, X. Y., Ma, J. B., Jiang, G. Q., Zhou, X. Q., & Shi, Q. (2017b). Formation of shallow water glaucony in weakly oxygenated Precambrian Ocean: An example from the Mesoproterozoic Tieling Formation in North China. *Precambrian Research, 294*, 214–229. https://doi.org/10.1016/j.precamres.2017.03.026

Thompson, G. R., & Hower, J. (1975). The mineralogy of glauconite. *Clays and Clay Minerals, 23*, 289–300. https://doi.org/10.1346/CCMN.1975.0230405

Tripathi, D. K., Singh, S., Singh, S., Mishra, S., Chauhan, D. K., & Dubey, N. K. (2015). Micronutrients and their diverse role in agricultural crops: advances and future prospective. *Acta Physiologiae Plantarum, 37*, 1–14.

Van Houten, F. B., & Purucker, M. E. (1984). Glauconitic peloids and chamositicooids — favorable factors, constraints, and problems. *Earth Science Reviews, 20*, 211–243. https://doi.org/10.1016/0012-8252(84)90002-3

Wigley, R., & Compton, J. S. (2007). Oligocene to Holocene glauconite-phosphorite grains from the Head of the Cape Canyon on the western margin of South Africa. *Deep Sea Research Part II: Topical Studies in Oceanography, 54*, 1375–1395. https://doi.org/10.1016/j.dsr2.2007.04.004

Wright, J., Schrader, H., & Holser, W. T. (1987). Paleoredox variations in ancient oceans recorded by rare-earth elements in fossil apatite. *Geochemica et Cosmochimica Acta, 51*, 631–644. https://doi.org/10.1016/j.dsr2.2007.04.004

Younes, H., Mahanna, H., & El-Etriby, H. K. (2019). Fast Adsorption of phosphate (PO_4^-) from wastewater using glauconite. *Water Science and Technology, 80*, 1643–1653. https://doi.org/10.2166/wst.2019.410